Structure, bandgap and optical properties of cubic $CsPbX_3$ (X = Cl, Br and I) under hydrostatic pressure

[1] Nawzad A. Abdulkareem and [2] Sarkawt A. Sami

[1] Department of Physics, College of Science, University of Zakho, Iraq
[2] Department of Physics, College of Science, University of Duhok, Iraq

Received: 26.06.2019

Abstract. In the recent years, caesium lead halides $CsPbX_3$ with the halogen elements Cl, Br and I have gained much attention of researchers owing to their attractive optical properties. In the present work we discuss the changes in their structure, bandgap and optical properties that occur under hydrostatic pressures 1–10 GPa. The density functional theory based on the generalized gradient approximation within the Perdew–Burke–Ernzerhof approach for exchange-correlation energy is used for calculations, in conjunction with the augmented plane-wave pseudopotential method. Since the generalized gradient approximation underestimates the bandgap, we employ the GW method to improve the bandgap values. The optical properties are computed in the photon-energy range 0.1–3.6 eV, using the density functional perturbation theory. As the pressure increases, the Pb–halogen bonds become contracted, whereas the volume of the unit cell shrinks uniformly, with no phase or structure-type transformations. The bandgap decreases with increasing pressure and the corresponding decrease rate for $CsPbI_3$ is less than that for $CsPbBr_3$. In general, the optical response of the caesium lead halides increases with increasing pressure, while the peaks of maximums of the response functions are red-shifted.

Keywords: $CsPbX_3$ perovskites, structure, induced optical properties, induced bandgap, *ab initio* calculations

UDC: 535.34

1. Introduction

All-inorganic perovskite compounds with a general formula ABX_3 have gained much attention of researchers owing to their strong response to electromagnetic radiation. Light emitting diodes [1, 2] and photodetectors [3] are among many applications of the ABX_3 compounds. In addition, their direct bandgap makes them promising for low-cost and high-efficiency solar cells. Formerly, the above materials have proved their high power-conversion efficiency, which has increased from 9.0% in 2012 up to 22.1% in 2016 [4, 5].

Among many inorganic perovskites, caesium lead halides (i.e., the compounds $CsPbX_3$ with X = Cl, Br and I, which are abbreviated hereafter as CLHs) are known as direct-bandgap semiconductors [6]. All of the three compounds reveal phase transformations. So, $CsPbBr_3$ has orthorhombic structure at the room temperature and undergoes a phase transition into a tetragonal phase at 88°C and into a cubic one at 130°C [7]. $CsPbCl_3$ undergoes a monoclinic-to-cubic phase transition at 47°C [8]. Finally, initially orthorhombic $CsPbI_3$ becomes cubic above 316°C [9].

A number of studies have dealt with the effect of pressure on the caesium lead halides. In particular, Geri et al. [10] have revealed a phase transition in $CsPbBr_3$ and $CsPbCl_3$ under the pressures up to 0.8 GPa at the room temperature. Zhang et al. [11] have proved the effect of pressure on the orthorhombic phase in $CsPbBr_3$, measured its optical properties experimentally

with a diamond-anvil cell method, and calculated the bandgap using the density functional theory. Zhang et al. [12] have studied the phase transition, the bandgap and the evolution of optical properties of the halide perovskite $CsPbCl_3$ upon compression. An orthorhombic-to-monoclinic phase transformation has been observed in $CsPbI_3$ at 3.9 GPa. It lasts up to the pressures 15 GPa [13]. Finally, Ilyas and Elias [14] have predicted theoretically that cubic $CsPbCl_3$ undergoes no phase transformation at the pressures up to 40 GPa.

This work focuses on the behaviour of structural, energy-band and optical properties of the cubic CLH perovskites under hydrostatic compression. The first-principles calculations based on the density functional theory are performed in order to predict the structure, bandgap and the optical characteristics of the $CsPbBr_3$, $CsPbCl_3$ and $CsPbI_3$ crystals subjected to hydrostatic pressures up to 10 GPa.

2. Computational techniques

The cubic perovskite ABX_3 structure has five atoms per unit cell. In the present work, these atoms are assumed to be located as follows: A at (0.0; 0.0; 0.0), B at (0.5; 0.5; 0.5) and X at (0.5; 0.5; 0.0), (0.5; 0.0; 0.5) and (0.0; 0.5; 0.5) (see Fig. 1). In our calculations we have used the density functional theory implemented with the Abinit package [15], in conjunction with the augmented plane-wave and norm-conserving pseudopotentials. We have employed norm-conserving, separable, dual-space Gaussian-type pseudopotentials by Goedecker, Teter and Hutter, as optimized for the generalized gradient approximation of the exchange-correlation functional by Perdew, Burke and Ernzerhof. The above approach considers the states $5s^2 5p^6 6s^1$ for Cs, $5d^{10} 6s^2 6p^2$ for Pb, $4s^2 4p^5$ for Br, $3s^2 3p^5$ for Cl and $5s^2 5p^5$ for I as valence states [16].

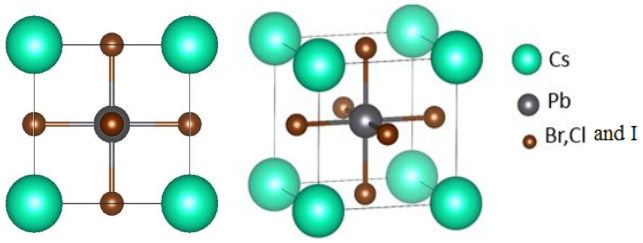

Fig. 1. Schematic structure of cubic $CsPbX_3$ perovskites.

At first, convergence calculations have been carried out. We have found that the acceptable convergence occurs with the plane-wave basis, the cut-off energy 1088 eV and the sampling of Brillouin zone based on the Monkhorst–Pack [17] k-point mesh of 6×6×6. We have applied the pressures 1–10 GPa to the unit cell of CLHs along all the directions. For each pressure, the system has been optimized structurally until the forces acting upon atoms are zero and the atoms are relaxed. This procedure is based upon the generalized gradient approximation of the density functional theory. Specifically, the Perdew–Burke–Erzornhof approach and the Kohn–Sham equation have been used to treat the exchange-correlation potential [18]. The optimized unit-cell dimensions (i.e., the lattice constant a) and the relaxed atomic coordinates have been taken to calculate the band structure and, hence, the bandgap, using the generalized gradient approximation within the approach by Perdew, Burke and Ernzerhof. The known GW method [19] has also been used to correct the fundamental bandgap values E_g. Real and imaginary parts of the dielectric function have been computed basing on the expressions derived with the density functional perturbation theory [20]. In addition, the real part of the refractive index and the absorption coefficient have been computed and used to interpret the response of our crystalline compounds to the visible light.

3. Results and discussion

3.1. Behaviour of structure

As mentioned above, the pressure has been applied homogenously to all sides of the cubic unit cell of the CLHs starting from 1 and finishing at 10 GPa. To predict structural response of our crystals to the hydrostatic pressure, the volume shrinkage and the contraction of Pb–halogen bond length are calculated. The main results are displayed in Fig. 2.

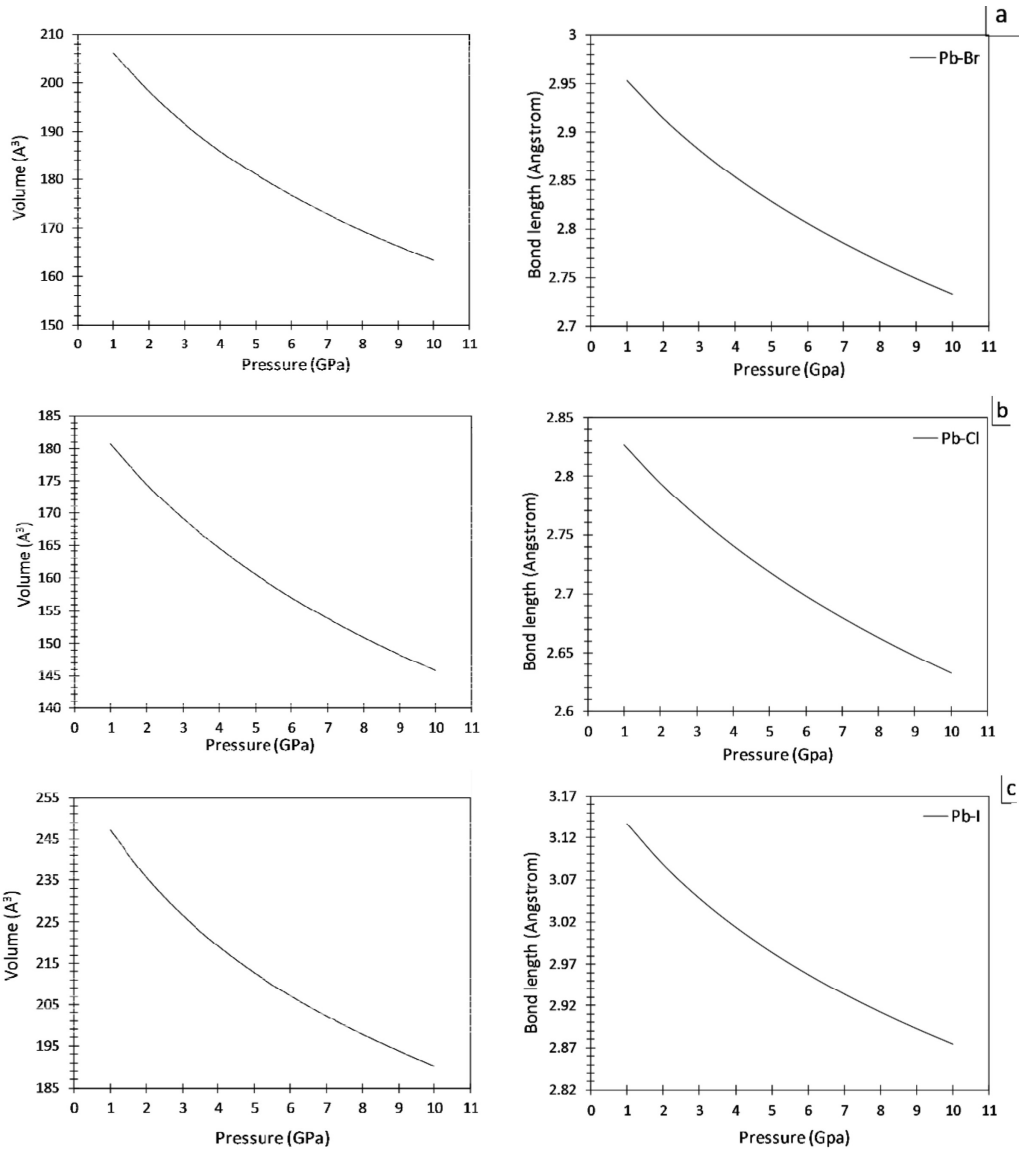

Fig. 2. Changes in the unit-cell volume (left panels) and Pb–halogen bond length (right panels) calculated for $CsPbBr_3$ (a), $CsPbCl_3$ (b) and $CsPbI_3$ (c) under compression.

No phase transformation is observed up to the maximal pressure of 10 GPa. As the pressure increases, the volume shrinks monotonously and the unit-cell dimensions are reduced homogenously (see the left panels in Fig. 2), whereas the bond lengths in the Pb–halogen network become shorter (see the right panels in Fig. 2). One can notice that the decrease in the unit-cell volume and in the Pb–halogen bond length slow down slightly as the pressure approaches to 10 GPa.

3.2. Bandgap values

The optimized lattice constants have been used to calculate the bandgaps E_g for the CLHs subjected to different pressures. This approach can offer a significant tool for tuning the optical properties of our crystals. The right panels in Fig. 3 show the pressure dependences of the bandgap at the high-symmetry points Γ, X, M and R in the first Brillion zone. The left panels display the pressure dependences of the energies that correspond to the top of the valence band and the bottom of the conduction band at the same symmetry points. This illustrates the contributions of these points into the effect of E_g tuning.

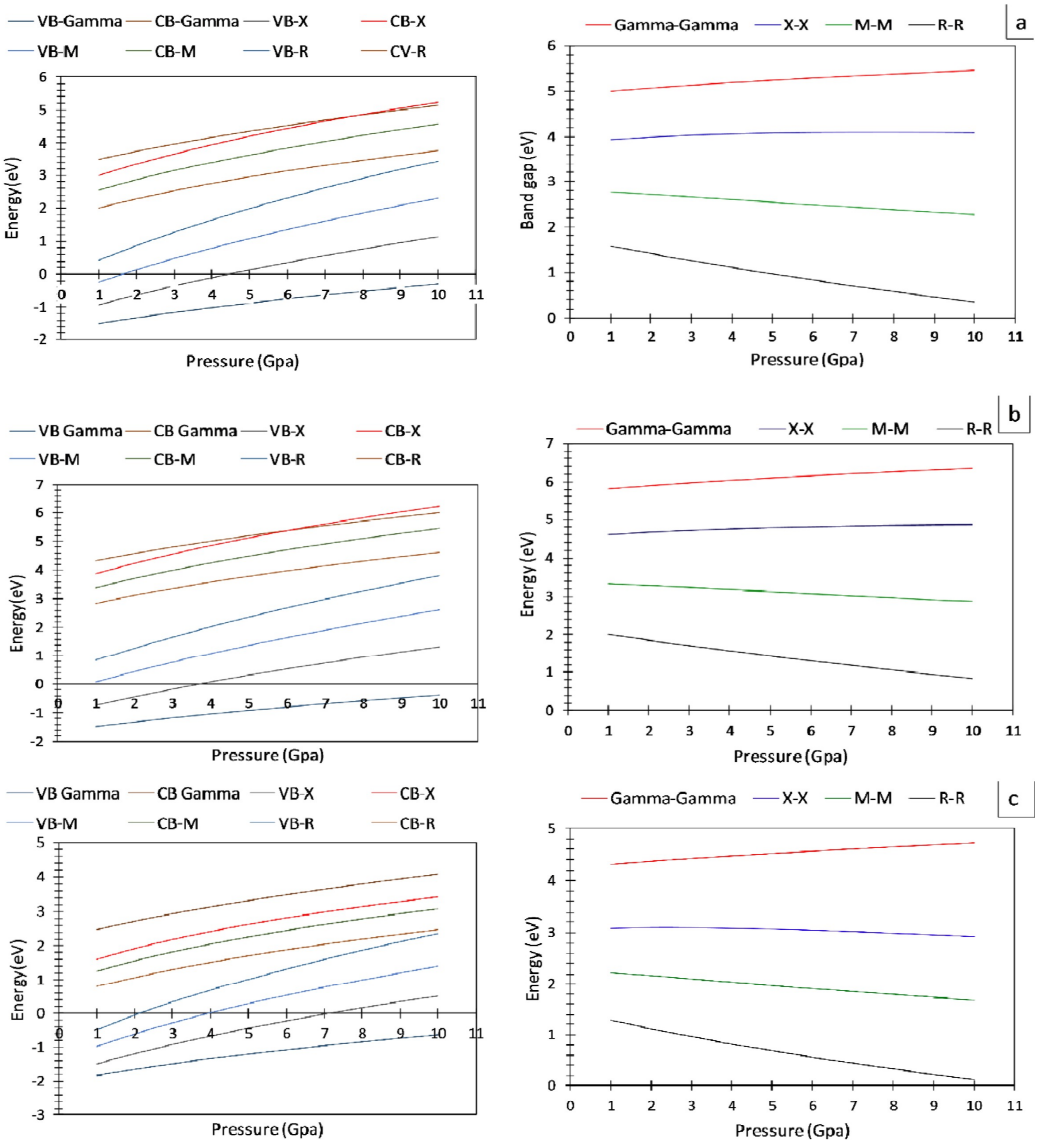

Fig. 3. Top of the valence band and bottom of the conduction band (left panels), and bandgaps (right panels) versus the hydrostatic pressure at different high-symmetry points, as calculated for $CsPbBr_3$ (a), $CsPbCl_3$ (b) and $CsPbI_3$ (c). The GW method is not employed to update the R-R gap (colour in online).

The bandgap values at the Γ and X points increase with increasing pressure. The appropriate pressure coefficients are 49.6 and 14.8 meV/GPa for $CsPbBr_3$, and 61 and 27.8 meV/GPa for

$CsPbCl_3$. For $CsPbI_3$, the bandgap increases at the Γ point and decreases at the X point. Here the pressure coefficients are 46.7 and –20.22 meV/GPa, respectively. The bandgap values decrease at the both points M and R. The relevant pressure coefficients are equal respectively to –57.1 and –136.9 meV/GPa for $CsPbBr_3$, –53.3 and –131.7 meV/GPa for $CsPbCl_3$, and –62.4 and –129.3 meV/GPa for $CsPbI_3$. The above figures testify that the bandgap values at the Γ, X and M points change only slightly with increasing pressure, while the bandgap at the R point undergoes somewhat larger changes. Hence, our results reveal that the bandgap at the R point is fundamental, which agrees well with the conclusions drawn in the earlier works.

The left panels in Fig. 3 demonstrate that the energy values corresponding to the top of the valence band and the bottom of the conduction band increase with increasing pressure at the high-symmetry points. However, our focus is the fundamental bandgap value, due to its significant role in optical transitions. It is clear from the left panels in Fig. 3 that, at the point R, the increase in the energy calculated for the top of the valence band is larger than that for the bottom of the conduction band. Obviously, this leads to narrower fundamental bandgap of the CLHs observed at higher pressures.

Due to a well-known bandgap problem of the density functional theory [21], the bandgap values calculated within the generalized gradient approximation of the Perdew–Burke–Ernzerhof method are underestimated. To overcome this problem, we have employed the GW method. The corrected fundamental bandgaps for the CLH compounds are displayed in Fig. 4.

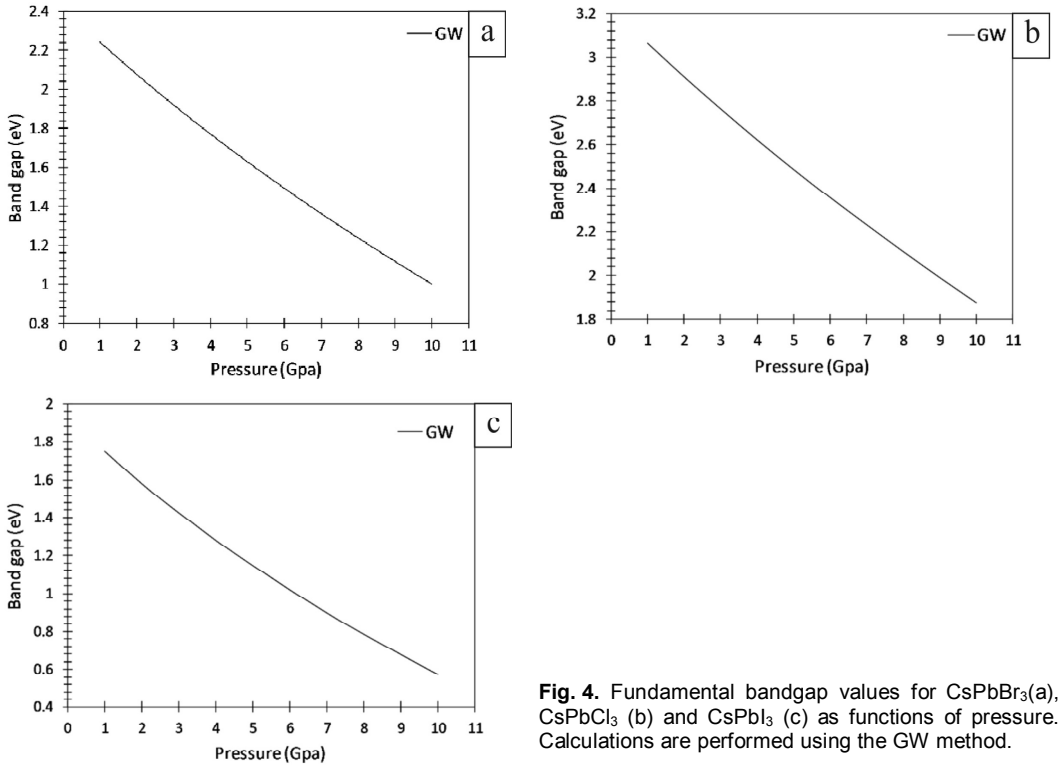

Fig. 4. Fundamental bandgap values for $CsPbBr_3$(a), $CsPbCl_3$ (b) and $CsPbI_3$ (c) as functions of pressure. Calculations are performed using the GW method.

As seen from Fig. 4, the fundamental bandgap E_g decreases with increasing pressure. As the pressure varies from 1 to 10 GPa, the absolute changes are equal to –1.23 eV for $CsPbBr_3$, –1.19 eV for $CsPbCl_3$ and –1.17 eV for $CsPbI_3$. This implies that $CsPbBr_3$ has the highest pressure sensitivity among the three compounds under analysis.

3.3. Optical properties

We have found the total optical response of the CLHs to electromagnetic radiation in the photon-energy region 0.1–3.6 eV, using the calculations of the pressure-modified complex dielectric function. The refractive index $n(\omega)$ and the absorption coefficient $\alpha(\omega)$ have also been calculated. Below we illustrate the main results obtained for our CLHs.

3.3.1. $CsPbBr_3$

The imaginary and real parts of the dielectric function, as well as the absorption coefficient and the refractive index for $CsPbBr_3$ are plotted against the photon energy in Fig. 5. At each pressure, the response fluctuates as the photon energy increases. In general, the calculated optical characteristics have nearly the same trend at all pressures. The increase in the pressure pushes the optical-response curves towards lower energies (a so-called red shift) and causes changes in their peak values (see Fig. 5).

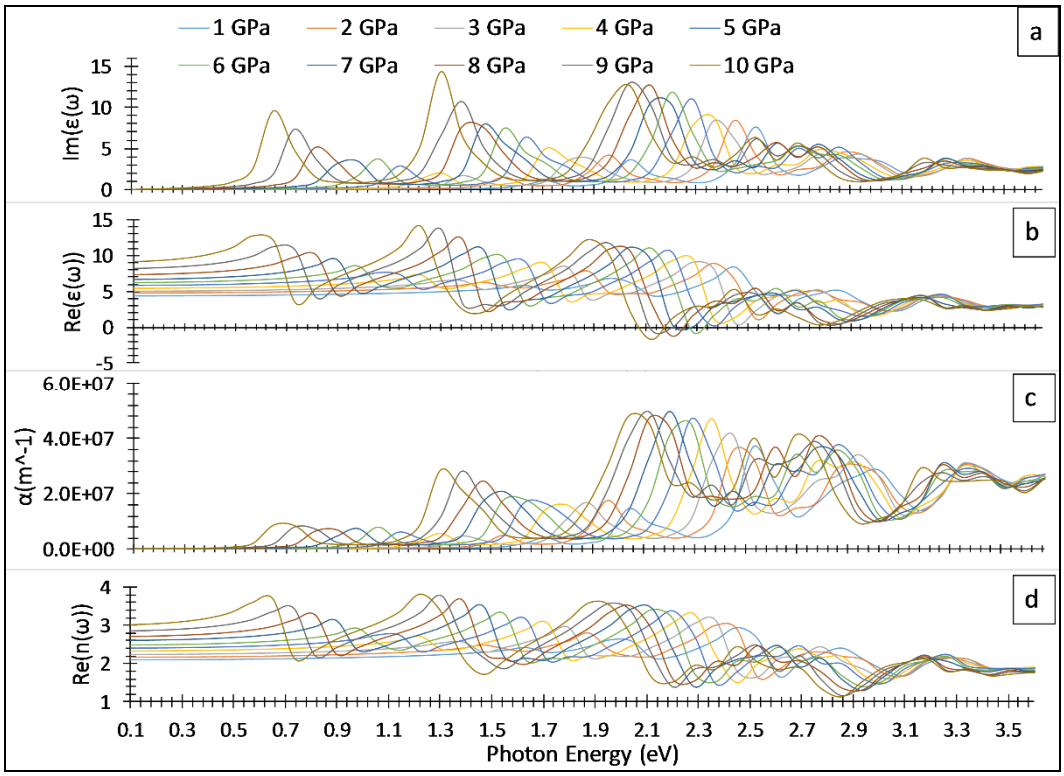

Fig. 5. Imaginary (a) and real (b) parts of the dielectric function, absorption coefficient (c) and refractive index (d) for $CsPbBr_3$ crystals at different hydrostatic pressures indicated in the legend (colour in online).

The imaginary part of the dielectric function varies with increasing pressure, while its maximum increases and shifts towards lower energies. The $\mathrm{Im}(\varepsilon(\omega))$ curve has a maximum at the photon energy 2.53 eV, which is acquired at 1 GPa and equals to 7.67. It still increases to 14.36 (being located at 1.3 eV) when the pressure is equal to 10 GPa. Thus, we have an increase of the peak response value and a red shift by 1.23 eV of the peak position.

The real part of the dielectric function $\mathrm{Re}(\varepsilon(\omega))$ has a maximum, 14.01, at 10 GPa which is reached at 1.22 eV. This value decreases with decreasing pressure, until it approaches the value

8.43 at 2.44 eV. In the similar way, the peak of the absorption coefficient increases and shifts towards lower energies when the pressure increases. Its values are equal to 4.7×10^7 and 3.7×10^7 m^{-1} when the pressures are 10 and 1 GPa, respectively. The behaviour of the refractive index is similar to that of the absorption coefficient. The maximal values of the refractive index at 10 and 1 GPa are respectively 3.80 and 2.95.

3.3.2. $CsPbCl_3$

Fig. 6 displays the changes in the linear optical properties for $CsPbCl_3$ occurring at different pressures. As with the $CsPbBr_3$ compound, here the maximal photon energy under test is equal to 3.6 eV. Quite similar to the case of $CsPbBr_3$, the optical response functions for the $CsPbCl_3$ crystals experience the fluctuations and trends with increasing pressure. In particular, the imaginary part of the dielectric function has the highest peak at the pressure 10 GPa. It equals to 12.95, being located at the photon energy 2.36 eV. The same parameters at 1 GPa amount to 6.02 and 2.93 eV. Hence, the red shift of the peak is 0.57 eV. The real part of the dielectric function, the absorption coefficient and the refractive index acquire their maximal values when the pressure is equal to 10 GPa.

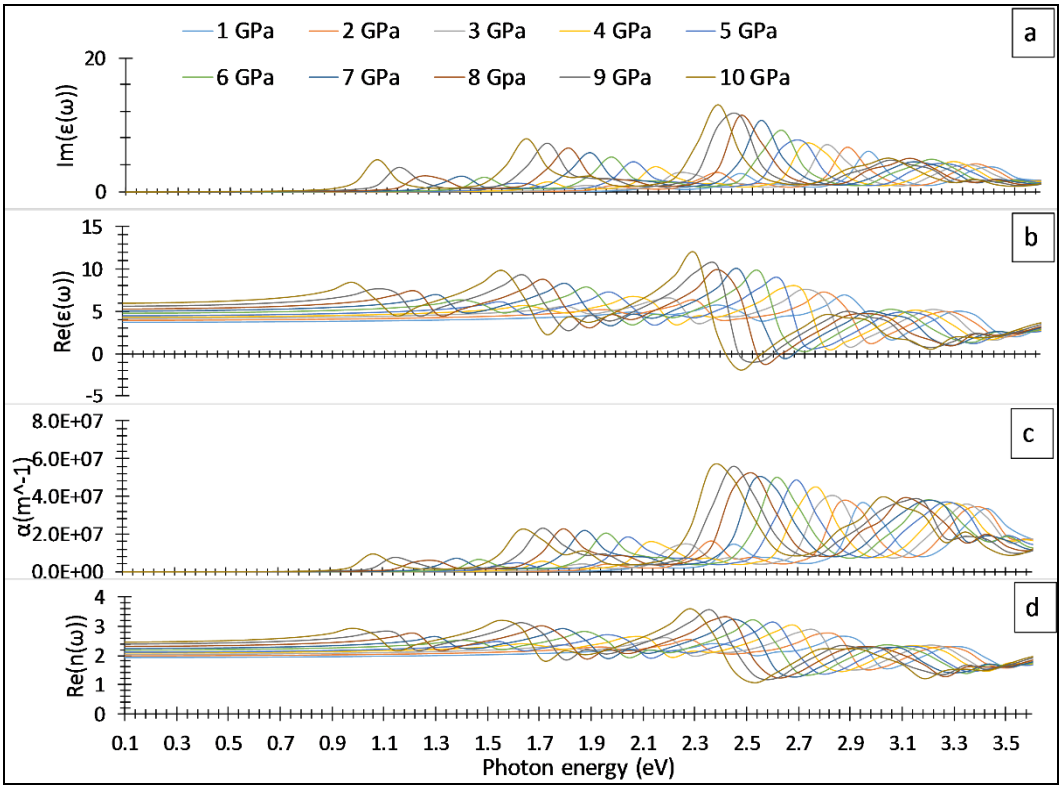

Fig. 6. Imaginary (a) and real (b) parts of the dielectric function, absorption coefficient (c) and refractive index (d) for $CsPbCl_3$ crystals at different hydrostatic pressures indicated in the legend (colour in online).

3.3.3. $CsPbI_3$

As with the $CsPbBr_3$ and $CsPbCl_3$ compounds, $CsPbI_3$ experiences fluctuations and trends of the optical functions with changing pressure. The imaginary and real parts of the dielectric function increase and shift towards lower photon energies when the pressure increases from 1 GPa to 10 GPa (see Fig. 7). For instance, the peaks of the imaginary part are shifted by 1.72 eV

when the pressure increases from 1 to 10 GPa. The absolute maximums of the absorption coefficient and the refractive index of $CsPbI_3$ at 10 GPa are equal to 4.14×10^7 m^{-1} and 4.29, respectively, while the absolute minimums occur at 1 GPa. They amount respectively to 3.38×10^7 m^{-1} and 3.04.

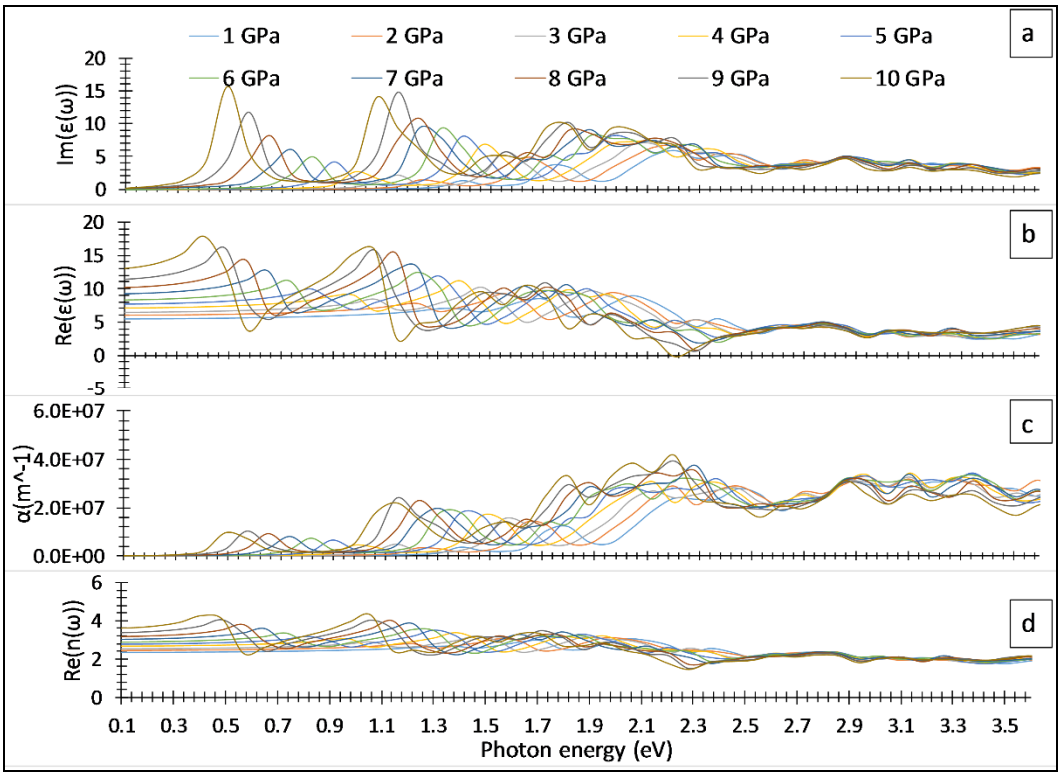

Fig. 7. Imaginary (a) and real (b) parts of the dielectric function, absorption coefficient (c) and refractive index (d) for $CsPbI_3$ crystals at different hydrostatic pressures indicated in the legend (colour in online).

4. Conclusions

The structures, the bandgaps and the optical characteristics of the cubic CLHs have been studied under hydrostatic pressures 1–10 GPa. For this aim we have used the well-known approach by Perdew and Wang in the frame of generalized gradient approximation of the density functional theory, the GW method, and the density functional perturbation theory.

We have demonstrated that none of the above materials experiences a phase transition under the pressure. The volume of the unit cell in the CLHs shrinks mainly due to contraction of the Pb–halogen bond lengths. The pressure coefficient of the volume contraction becomes less with increasing pressure. When the pressure increases, the bandgap values also decrease. The pressure rate of this process is reduced if one passes from Br to I.

In general, the optical response of our materials becomes stronger with increasing pressure. The maximums of the imaginary and real parts of the dielectric function are then shifted down to the energies lower than 1.5 eV, which corresponds to the infrared range. The pressure changes in the imaginary part of the dielectric function are not the same for all of the three compounds. For example, the peaks corresponding to maximums are shifted towards lower energies by 0.57, 1.23 and 1.72 eV respectively for $CsPbCl_3$, $CsPbBr_3$ and $CsPbI_3$, as the pressure increases from 1 to 10 GPa. The wider the bandgap of the material the less the corresponding shift is.

Issuing from the data obtained in the present work, one can witness a significant effect of hydrostatic pressure on the materials under study. Finally, our results can be important for predicting and improving both the electronic and optical properties of the cubic CLHs.

References

1. Tan Z-K, Moghaddam R S, Lai M L, Docampo P, Higler R, Deschler F, Price M, Sadhanala A, Pazos, L M, Credgington D, Hanusch F, Bein T, Snaith H J and Friend R H, 2014. Bright light-emitting diodes based on organometal halide perovskite. Nature Nanotechnol. **9**: 687–692.
2. Song J, Li J, Li X, Xu L, Dong Y and Zeng H, 2015. Quantum dot light-emitting diodes based on inorganic perovskite cesium lead halides ($CsPbX_3$). Adv. Mater. **27**: 7162–7167.
3. Wei H, Fang Y, Mulligan P, Chuirazzi W, Fang H-H, Wang C, Ecker B R, Gao Y, Loi M A, Cao L and Huang J, 2016. Sensitive X-ray detectors made of methylammonium lead tribromide perovskite single crystals. Nature Photonics. **10**: 333–339.
4. Kim H S, Lee C R, Im J H, Lee K B, Moehl T, Marchioro A, Moon S J, Humphry-Baker R, Yum J H, Moser J E, Grätzel M and Park N G, 2012. Lead iodide perovskite sensitized all-solid-state submicron thin film mesoscopic solar cell with efficiency exceeding 9%. Sci. Rep. **2**: 591.
5. Mutalikdesai A and Ramasesha S K, 2017. Emerging solar technologies: Perovskite solar cell. Resonance. **22**: 1061–1083.
6. Chang Y H and Park C H, 2004. First-principles study of the structural and the electronic properties of the lead-halide-based inorganic-organic perovskites (CH_3NH_3) PbX_3 and $CsPbX_3$ (X = Cl, Br, I). J. Korean Phys. Soc. **44**: 889–893.
7. Stoumpos C C, Malliakas C D, Peters J A Liu Z, Sebastian M, Im J, Chasapis T C, Wibowo A C, Chung D Y, Freeman A J, Wessels B W and Kanatzidis M G, 2013. Crystal growth of the perovskite semiconductor $CsPbBr_3$: a new material for high-energy radiation detection. Cryst. Growth Des. **13**: 2722–2727.
8. Møller Chr Kn, 1958. Crystal structure and photoconductivity of cæsium plumbohalides. Nature. **182**: 1436.
9. Sharma S, Weiden N and Weiss A, 1992. Phase diagrams of quasibinary systems of the type: $ABX_3 – A'BX_3$; $ABX_3 – AB'X_3$, and $ABX_3 – ABX'_3$; X = Halogen. Z. Phys. Chem. **175**: 63–80.
10. Gesi K, Ozawa K and Hirotsu S, 1975. Effect of hydrostatic pressure on the structural phase transitions in $CsPbCl_3$ and $CsPbBr_3$. J. Phys. Soc. Japan. **38**: 463–466.
11. Long Zhang, Qingxin Zeng and Kai Wang, 2017. Pressure-induced structural and optical properties of inorganic halide perovskite $CsPbBr_3$. J. Phys. Chem. Lett. **8**: 3752–3758**.**
12. Long Zhang, Lingrui Wang, Kai Wang and Bo Zou, 2018. Pressure-induced structural evolution and optical properties of metal halide perovskite $CsPbCl_3$. J. Phys. Chem. C. **122**: 15220–15225.
13. Guan Yuan, Shan Qin, Xiang Wu, Hongrui Ding and Anhuai Lu, Pressure-induced phase transformation of $CsPbI_3$ by X-ray diffraction and Raman spectroscopy. Phase Trans. **91**: 38–47.
14. Bahaa M Ilyas and Badal H Elias, 2017. A theoretical study of perovskite CsXCl3 (X=Pb, Cd) within first principles calculations. Physica B. **510**: 60–73.
15. Gonze X, Amadon B, Anglade P M, Beuken J-M, Bottin F, Boulangera P, Bruneval F, Calistej D, Caracas R, Cote M, Deutsch T, Genovese L, Ghosez Ph, Giantomassi M,

Goedecker S, Hamann D R, Hermet P, Jollet F, Jomard G, Leroux S, Mancini M, Mazevet S, Oliveira M J T, Onida G, Pouillon Y, Rangel T, Rignanese G-M, Sangalli D, Shaltaf R, Torrentd M, Verstraete M J, Zerah G and Zwanziger J W, 2009. ABINIT: First-principles approach to material and nanosystem properties. Comput. Phys. Commun. **180**: 2582–2615.

16. Krack M, 2005. Pseudopotentials for H to Kr optimized for gradient-corrected exchange-correlation functionals. Theor. Chem. Acc. **114**: 145–152.
17. Monkhorst H J and Pack J D, 1976. Special points for Brillouin-zone integrations. Phys. Rev. B. **13**: 5188–5192.
18. Perdew J P, Burke K and Ernzerhof M, 1996. Generalized gradient approximation made simple. Phys. Rev. Lett. **77**: 3865–3868.
19. Hedin L, 1965. New method for calculating the one-particle Green's function with application to the electron-gas problem. Phys. Rev. **139**: A796–A823.
20. Sharma S and Ambrosch-Draxl C, 2004. Second-harmonic optical response from first principles. Phys. Scripta. **2004**: T109.
21. Perdew J P, 1985. Density functional theory and the band gap problem. Int. J. Quant. Chem. **28**: 497–523.

Nawzad A. Abdulkareem and Sarkawt A. Sami. 2019 Structure, bandgap and optical properties of cubic $CsPbX_3$ halides (X = Cl, Br and I) under hydrostatic pressure. Ukr.J.Phys.Opt. **20**: 132 - 141. doi: 10.3116/16091833/20/3/132/2019

Анотація. *В останні роки свинцевовмісні галогеніди цезію $CsPbX_3$ з елементами галогенів Cl, Br та I привертають значну увагу дослідників завдяки привабливим оптичним властивостям. У цій роботі обговорено зміни в їхній структурі, ширині забороненої зони та оптичних властивостях, які з'являються під гідростатичними тисками 1–10 ГПа. У розрахунках використано теорію функціонала густини, що ґрунтується на узагальненому градієнтному наближенні в рамках підходу Пердью–Бурке–Ернцергофа для обмінно-кореляційної енергії, разом із методом розширеного плоскохвильового псевдопотенціалу. Оскільки узагальнене градієнтне наближення недооцінює ширину забороненої зони, для поліпшення розрахунків ми застосували відомий метод GW. Оптичні властивості обчислено в діапазоні фотонних енергій 0,1–3,6 еВ на основі теорії збурень для функціонала густини. Показано, що зі зростанням тиску зв'язки Pb–галоген скорочуються, тоді як об'єм елементарної комірки однорідно зменшується, без жодних фазових перетворень або змін структурного типу. За цих же умов заборонена зона звужується, а відповідна швидкість її звуження для сполуки $CsPbI_3$ менша, ніж для $CsPbBr_3$. Загалом зростання тиску приводить до посилення оптичного відгуку свинцевовмісних галогенідів цезію, а піки максимумів їхніх функцій відгуку зазнають червоного зсуву.*